RESEARCH ARTICLE

ADVANCED
INTELLIGENT
SYSTEMS
Open Access

www.advintellsyst.com

Phase Stability in Rare-Earth-Doped Apatites: A Machine Learning Approach

Geeta Sharma,* Sarathkumar Loganathan, Evangelos Daskalakis, Eric K. Barimah, Simon Strafford, and Animesh Jha

The study examines thermal behavior and phase stability of rare-earth-doped apatites (cerium, samarium, and holmium ions) between 25 °C and 1200 °C. Decomposition and thermal-induced phase transitions are analyzed by in situ high-temperature X-ray diffraction (HT-XRD) and thermogravimetric analysis (TGA). Decision tree machine learning (ML) model is developed to predict phase stability and decomposition products as a function of composition and temperature. The feature importance analysis identifies temperature as the determining factor for phase stability. The correlation heatmap shows strong correlation between temperatures above 600 °C and phase instability. The model achieves an accuracy of $\approx$86%, classified into three thermal regimes: 1) single-phase stable behavior below 500 °C, 2) partial decomposition between 500 °C and 800 °C with formation of β-tricalcium phosphate (β-TCP) and oxyapatite, and 3) complete transformation above 800 °C into α-TCP and Sr/Ca-apatite phases. Cerium and samarium ion doping improve stability up to 600 °C by reducing vacancy formation, whereas co-doping with holmium ion triggers earlier decomposition ($\approx$500 °C) due to increased lattice strain. ML-based framework reduces need for large-scale experimental screening, enhances research efficiency and offers predictive in silico tool to design thermally stable apatite-based materials for biomedical and catalytic applications.

1. Introduction

The apatite subgroup represented by chemical formula $^{IX}M1_2 {}^{VII}M2_3 (^{IV}TO_4)_3X$[1,2] is an ensemble of materials possessing high structural and compositional flexibility.[3] The apatite subgroup consisting of phosphates, arsenates, vanadates, silicates, and sulfates, each offering unique properties that make them suitable for diverse applications, for example, biomedicine

G. Sharma, S. Loganathan, E. Daskalakis, E. K. Barimah, S. Strafford, A. Jha
Faculty of Engineering and Physical Sciences
School of Chemical and Process Engineering
University of Leeds
Leeds LS2 9JT, UK
E-mail: g.sharma@leeds.ac.uk

The ORCID identification number(s) for the author(s) of this article can be found under https://doi.org/10.1002/aisy.202500293.

and catalysis.[4–6] The apatites crystallizes in the $P6_3/m$ space group; however, the deviation from the original group may occur frequently due to cation ordering, resulting in more complex structural variations. Apatite structure owes the versatility to their ability to accommodate a range of ions in their crystal structure.[7] In the apatite structure, the M-site can be hosted by divalent and trivalent cations such as Mn^{2+}, Y^{3+}, Ba^{2+}, Ce^{3+}, Na^+, Sr^{2+}, Pb^{2+}, La^{3+}, Ca^{2+}, and Bi^{3+}. The higher valency cations such as Si^{4+}, P^{5+}, V^{5+}, S^{6+}, and As^{5+} can be present at the T-site,[8] while the anions such as F^-, $(OH)^-$, and Cl^- often occupy the X-site.[9] Doping apatite-based materials with rare-earth ions is a widely used method to tailor their properties, including improved thermal stability, optical performance, magnetic behavior, and catalytic efficiency.[3,10] Rare-earth ions, because of $4f$ electronic configurations, introduce localized distortions in the crystal lattice, changing bond lengths and angles.[11] Changes in the dimensions and angles of apatite materials alter their physicochemical characteristics, which in turn influence bond strength, atomic arrangement, and crystal symmetry. These modifications impact solubility by altering ion mobility and mechanical properties by affecting structural rigidity. They also influence bioactivity by changing surface charge and chemical reactivity.[12] It is extremely essential to identify and optimize the phase stability of rare-earth ion-doped apatite in different thermal conditions. Phase stability has a significant impact on the solubility of apatite, mechanical properties, and bioactivity.[13] Temperature-driven phase transformations may result in ion migration or deformation of the lattice.[7,14,15] Such information is critical in applications of rare-earth-doped apatites in waste treatment, lighting, and biomaterials, where high-temperature treatment is demanded.[16–18]

In an earlier report, we investigated the phase transformation properties of rare-earth-doped apatite structures containing cerium, samarium, and holmium ions across a broad temperature range (25–1200 °C).[3] By employing advanced characterization techniques such as in situ high-temperature X-ray diffraction (HT-XRD), thermogravimetric analysis (TGA), X-ray photoelectron spectroscopy (XPS), and Fourier-transform infrared spectroscopy (FTIR), we studied the structural evolution, thermal expansion

**ADVANCED
SCIENCE NEWS**

www.advancedsciencenews.com

**ADVANCED
INTELLIGENT
SYSTEMS**
Open Access

www.advintellsyst.com

behavior, and decomposition mechanisms of apatite materials. It was shown that the temperature dependence of phase decomposition is dependent on the type and site occupied in $P6_3/m$ by the RE^{3+}-ions and their concentrations in the lattice structure of apatite.[3]

Based on previously published experimental data,[3] we here describe a machine learning (ML) approach for predicting the phase stability and decomposition tendencies of rare-earth ion doped apatite structures across a wide temperature range (25–1200 °C). ML in materials science has transformed the ability to generate rapid predictions. It augments experiments by deriving patterns and relationships from high-dimensional data.[19–21] This work uses ML to model the stability and decomposition behavior of cerium ion, samarium ion, and holmium ion-doped apatite materials. A decision tree model is developed to predict stable phases, decomposition temperatures, and products for the following four compositions: fluoroapatite (FA); Ce^{3+}-doped FA (FACe); Ce^{3+} and Sm^{3+} co-doped FA (FACeSm); and Ce^{3+}, Sm^{3+}, and Ho^{3+} co-doped FA (FACeSmHo). The model achieves an accuracy of around 86%, detecting important transition points such as the onset of instability and development of multi-phase products. Temperature is identified as the key factor influencing phase stability in the feature-only analysis. The ML model framework reduces the need for extensive experimental screening at large scales by finding key transition points like nucleation of multiple phases and instability onset. The predictive modeling of biominerals can be used to give insights into phase transformation in vivo, e.g., osseointegration of dental implants and bone remodeling. This work shows the capability of ML-assisted materials science in designing rare-earth-doped apatite structure.

2. Experimental Section

2.1. Synthesis of Apatites

The sol–gel process was used to synthesize OH-containing fluorapatite doped with 2 mole% strontium and rare-earth elements.[3] The host matrix was doped with 2 mole% Ce^{3+} for Ca^{2+} and 2 mole% of PO_{4-} substituted with F^-. To examine the influence of the increased concentration of doping on the structural aspects, apatite compositions thus prepared were double and triple-doped with other rare-earth ions (Sm^{3+} and Ho^{3+}). Four different compositions were produced, namely $Ca_{4.98}Sr_{0.02}(PO_4)_3$ $OH_{0.98}F_{0.02}$, $Ca_{4.96}Sr_{0.02}Ce_{0.02}(PO_4)_3OH_{0.98}F_{0.02}$, $Ca_{4.95}Sr_{0.02}$ $Ce_{0.02}Sm_{0.01}(PO_4)_3OH_{0.98}F_{0.02}$, and $Ca_{4.94}Sr_{0.02}Ce_{0.02}Sm_{0.01}Ho_{0.01}$ $(PO_4)_3OH_{0.98}F_{0.02}$ (referred to as FA, FACe, FACeSm, and FACeSmHo, respectively). The detail of synthesis procedure is reported elsewhere.[3]

2.2. Experimental Methods

In situ HT-XRD analysis was used to investigate high-temperature phase transitions. An Anton Paar HTK 1200 N high-temperature chamber equipped with a Panalytical X'Pert Pro powder diffractometer was used for the investigations. In increments of 50 °C, the temperature was raised from ambient temperature (25 °C) to 1200 °C. XRD scans were recorded within the 20°–70° range, using a scan step of 0.013°. The synthesized materials closely matched the reference XRD data for fluorapatite, confirming the presence of an OH^-/F^--substituted crystal structure (ICDD: 04-015-6661). A simultaneous thermal analyzer (PerkinElmer STA 8000) with TGA capabilities was used to further study the decomposition behavior of apatite and related phase transitions following heating in an air atmosphere. Over a temperature range of 25–1200 °C, thermal measurements were carried out in alumina crucibles at a heating rate of 10 °C min^{-1}.

2.3. Data Collection

The HT-XRD was used to examine the phase decomposition behavior of the four apatite materials (FA, FACe, FACeSm, and FACeSmHo). The Rietveld refinement was used to analyze the XRD pattern for identification of phases and their evolution across the temperature range studied (25–1200 °C). The findings provided information on the thermal stability of each composition by revealing temperature-sensitive phase transitions as well as the emergence of new phases. The XRD results were in agreement with the TGA results. Using XRD data, a structured dataset was produced that included transition temperatures, phase stability, and the number of different phases. This dataset served as input for training ML model. The ML algorithm was used to identify the key patterns in the structural evolution of the materials, which were used to design a predictive model. The model forecasted phase changes as a function of temperature and composition. The approach describes the potential of combining ML with the experimental study to accelerate the finding of thermally stable apatite-based materials.

2.4. ML and Modeling

The ML method was used to develop a decision tree model due to its well-defined structure, interpretability, and visualizability.[22,23] Other models were also tested, including K-nearest neighbors (kNN).[24,25] However, kNN achieved an accuracy of only 37%. Therefore, the decision tree model was opted. Across the temperature range of 25–1200 °C, the decision tree model examined the key factors affecting the stability and product formation of four apatite materials. The analysis specifically focused on two main parameters: temperature and material composition, which determined the outputs related to stability (classified as stable or unstable), products, and number of products formed. As temperature increased, each material's behavior was categorized into distinct phases of stability, followed by the decomposition into multiphase products at higher temperatures. The materials investigated included FA, FACe, FACeSm, and FACeSmHo, which were encoded in the model as 0, 1, 2, and 3, respectively. Stable and unstable products were labeled as 0 and 1. **Table 1** and **2** list the encoding scheme for classification labels and abbreviations of decomposition products respectively.

The dataset comprised 100 samples, which were split into features (X) and target variables (y), where "ABBR" represented the classification of different phases. The train_test_split function was used to split the dataset into an 80% training set and a 20% testing set for model training. A DecisionTreeClassifier was then fitted to the training data, learning to classify material behavior based on the input features. The model achieved ≈86%

**ADVANCED
SCIENCE NEWS**

www.advancedsciencenews.com

**ADVANCED
INTELLIGENT
SYSTEMS**

www.advintellsyst.com

Table 1. Label encoding scheme for material stability classification and doped material types in the apatite system.

Label value	Description	Target variable
Stability classification		
0	Stable	Material stability
1	Unstable	Material stability
Material composition classification		
0	FA (base material)	Material type
1	FACe (FA cerium ion doped)	Material type
2	FACeSm (FA cerium and samarium ion doped)	Material type
3	FACeSmHo (FA cerium, samarium, and holmium ion doped)	Material type

Table 2. Abbreviations of decomposition products.

Abbreviation (ABBR)	Chemical formula	Product name
FA with water loss	Oxyapatite	Oxyapatite
αTCP	$\alpha\text{-}Ca_3(PO_4)_2$	α-Tricalcium phosphate
βTCP	$\beta\text{-}Ca_3(PO_4)_2$	β-Tricalcium phosphate
TTCP	$Ca_4P_2O_9$	Tetra calcium phosphate
CaSrAP	$Ca_{9.37}Sr_{0.63}(PO_4)_6(OH)_{0.98-2x}F_{0.02}O_x$	Calcium-strontium apatite
SrCaAP	$Sr_{7.3}Ca_{2.7}(PO_4)_6(OH)_{0.98-2x}F_{0.02}O_x$	Strontium-calcium apatite

accuracy on the test set as calculated with the accuracy_score function. In order to evaluate the model robustness and prevent overfitting, the training set was subjected to a five-fold cross-validation. In this process, the data was split into five subsets: four were used to train the model, and one was used for validation. The method was repeated five times with each subset being used for validation once. The accuracy values obtained across the folds were [1.00, 1.00, 1.00, 0.95, 1.00], with an average accuracy of 0.99. The results indicate that the model performed well for all the various partitions of the data, which validates its robustness. The method also helps in reducing bias and variance, encouraging better generalization to new data. Feature importance analysis of the decision tree confirmed that temperature was the primary driver towards material stability accounting for 89% of the explanatory power, whereas the material type contributed only 11%.[26] This finding was also validated through a correlation heatmap[27] that indicated strong positive correlation of temperature values above 600 °C and instability across all the materials, with simultaneous capture of material-specific effects on product formation at high temperatures.

3. Results and Discussion

3.1. Material Phase Analysis at Various Temperatures

The XRD patterns show characteristic diffraction peaks corresponding to ICDD no. 04–015-6661, confirming a hexagonal crystal structure ($P6_3/m$) (**Figure 1**). The phase decomposition behavior of the apatite lattice doped with rare-earth ions was analyzed between temperature 25–1200 °C using in situ high-temperature powder XRD. Figure S1–S5, Supporting Information, present the high-temperature XRD patterns for undoped FA, FACe, FACeSm, and FACeSmHo are in the supplementary section. The phase decomposition behavior aligns well with thermal analysis results, with thermal analysis results detailed in Figure S6, Supporting Information. XPS spectroscopy confirmed the presence of dopants and their oxidation states. The cerium and samarium ions existed in multiple oxidation states (Ce^{3+}, Ce^{4+}, Sm^{3+}, Sm^{2+}), while holmium was found exclusively in the Ho^{3+} state (reported elsewhere).[3] All the samples exhibit two clearly differentiated zones, a stable phase initially followed by phase instability, in which several decomposition products appear at various temperatures. Rare-earth ion substitution affects the apatite lattice's vacancy creation, changing the breakdown processes, byproducts, and the fraction of tri-calcium phosphate formed.[3] Determining the stability range and decomposition pathways for these materials remains a complex task. To predict phase stability and better understand the decomposition pathways, ML was employed to analyze the dataset derived from HT-XRD and thermal analysis.

3.2. Thermal Behavior of Apatite Materials

Figure 2 is a box plot of the thermal response of FA, FACe, FACeSm, and FACeSmHo, designated 0, 1, 2, and 3,
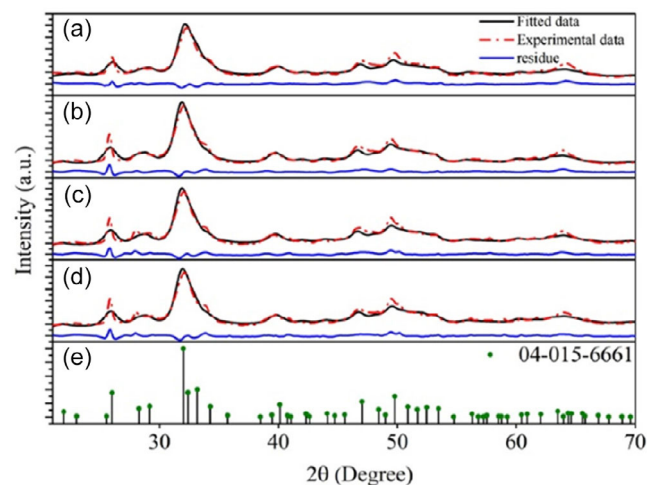

Figure 1. Powder X-ray diffraction patterns at room temperature for a) FA, b) FACe, c) FACeSm, and d) FACeSmHo show characteristic diffraction peaks corresponding to the hexagonal apatite structure, compared with the e) standard data ICDD 04–015-6661. The incorporation of dopants result in shifts in peak positions and changes in intensities, suggesting slight lattice distortions due to ionic substitution.
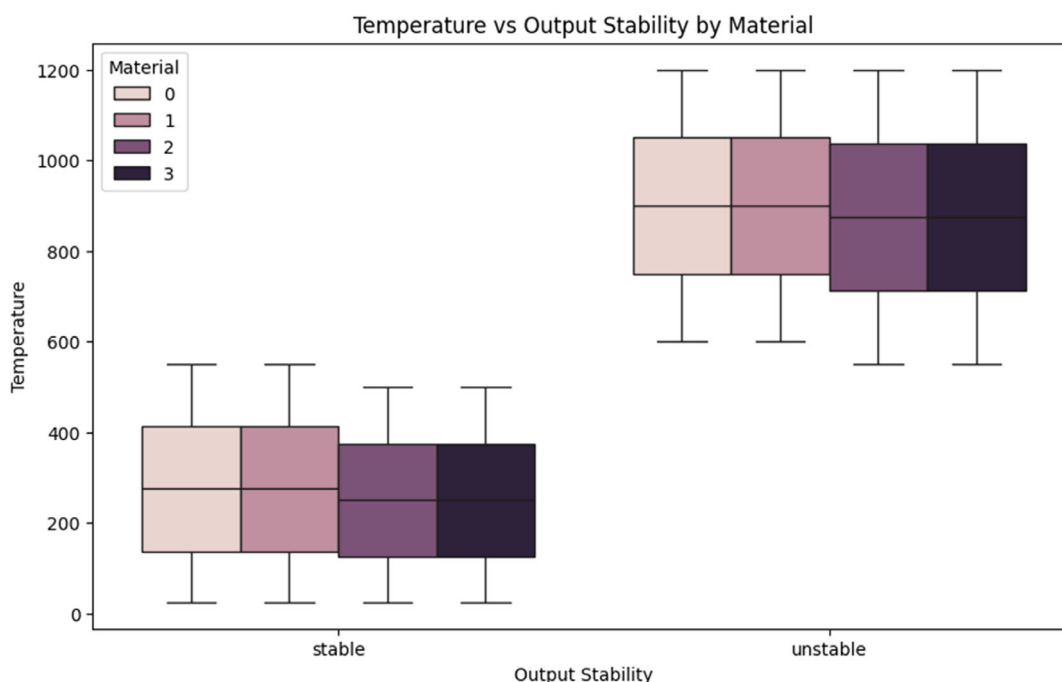
Figure 2. Box plot comparing the thermal stability of four materials—FA, FACe, FACeSm, and FACeSmHo (labeled as 0, 1, 2, and 3, respectively)—from 25 °C to 1200 °C. Stability of each material is labelled as "stable" or "unstable," representing the effect of rare-earth doping on phase transition and decomposition characteristics. The plot shows data at the temperature points where each material undergoes a transition from stable to unstable phase.

respectively, for the temperature range of 25–1200 °C The x-axis indicates the stability regimes, denoted as "stable" and "unstable," and the y-axis represents the temperature. Materials 0, 1, and 3 remain stable until around 500 °C, whereas material 2 is more thermal-resistant by being stable up to around 600 °C. All the materials destabilize at temperatures above these, where materials 2 and 3 decompose faster than materials 0 and 1 beyond 600 °C. The breakdown of the materials is influenced by the oxidation state of the rare-earth ions substituted in the apatite lattice.[3] **Figure 3** shows the decision tree feature importance analysis. It identifies the temperature as the primary factor for material stability. Temperature is accounting for 89% of the predictive power whereas material type is responsible for 11% only. The finding is supported by the correlation heat map shown in **Figure 4**. The material type and temperature versus product
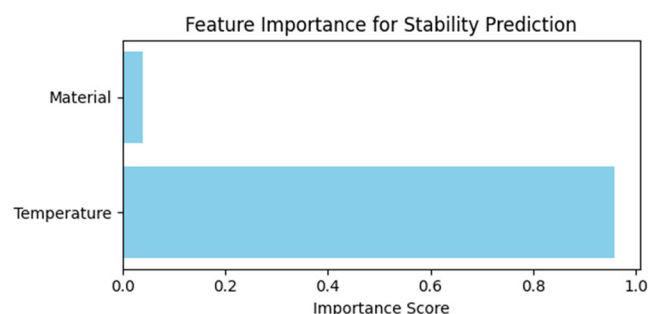
formation correlation plot is shown in Figure 4a,b. It is evident from Figure 4a that α-TCP demonstrates a strong positive correlation ($r = 0.78$) with temperature range 901–1200 °C, demonstrating that its formation is favored at high temperatures. Similarly, β-TCP and SrCaAP exhibit moderate correlations with mid-to-high temperature ranges (601–900 °C and 901–1200 °C), corresponding to temperature-induced phase formation. In contrast, CaSrAP and SrCaAP have negative correlation with low temperatures and shows no formation at 25–300 °C. The material type also affects the product phases and is plotted in Figure 4b. Although most materials exhibit weak correlations, FACeSmHo composition shows a moderate positive correlation ($r = 0.40$) with TTCP formation, which indicates that certain rare-earth dopants can influence certain phase formations. Temperature is the main determinant when instability occurs, dopant selection significantly influences which decomposition products forms.

The decision tree model was used to predict the stability and behavior of decomposition of rare-earth-doped apatite materials (FA, FACe, FACeSm, and FACeSmHo) based on composition and temperature. Temperature (continuous variable) and composition of material (categorical variable with values 0, 1, 2, and 3 for various materials) are input variables. Phase stability and decomposition products are the coveted outputs of the model. Terminal leaves are for temperature or material composition-based decisions, and internal nodes are for predicted outcomes. The model can detect the most severe change points, i.e., where a phase degraded to many products or destabilized, by a temperature value. The observation led to the fact that material composition and temperature played a strong controlling role
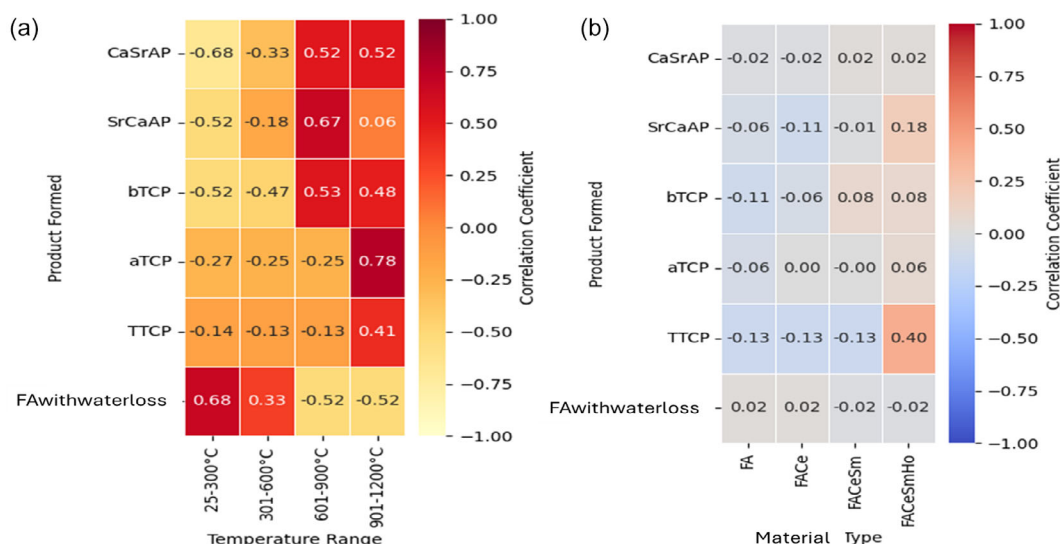

Figure 3. Feature importance plot showing that temperature is the primary factor influencing product formation, while material type has minimal impact.

Figure 4. a) Correlation heatmap showing the correlation coefficients between temperature ranges and the formation of different products. Strong positive correlations (e.g., α-TCP at 901–1200 °C, $r = 0.78$) suggest thermally favored phases, while negative correlations (e.g., CaSrAP at 25–300 °C, $r = -0.68$) indicate suppression at lower temperatures. The FAwithwaterloss product favors lower temperatures by a distinct margin and b) heatmap of the correlation between different types of dopants (material compositions) and product formation. While material-product correlations in general are weak, FACeSmHo shows a strong positive correlation ($r = 0.40$) with TTCP formation, suggesting that specific dopants can trigger the formation of certain phases.

in managing phase transformation, especially at temperatures of 500 °C and above. **Figure 5** shows the decision tree indicating influence of temperature on material stability and product development and how dopants can affect material responses.

In lower temperatures (25–550 °C), the apatite materials are stable and exist in single phase. All the four materials—material 0 (FA), material 1 (FACe), material 2 (FACeSm), and material 3 (FACeSmHo)—are stable at temperature up to 50 °C. Above this
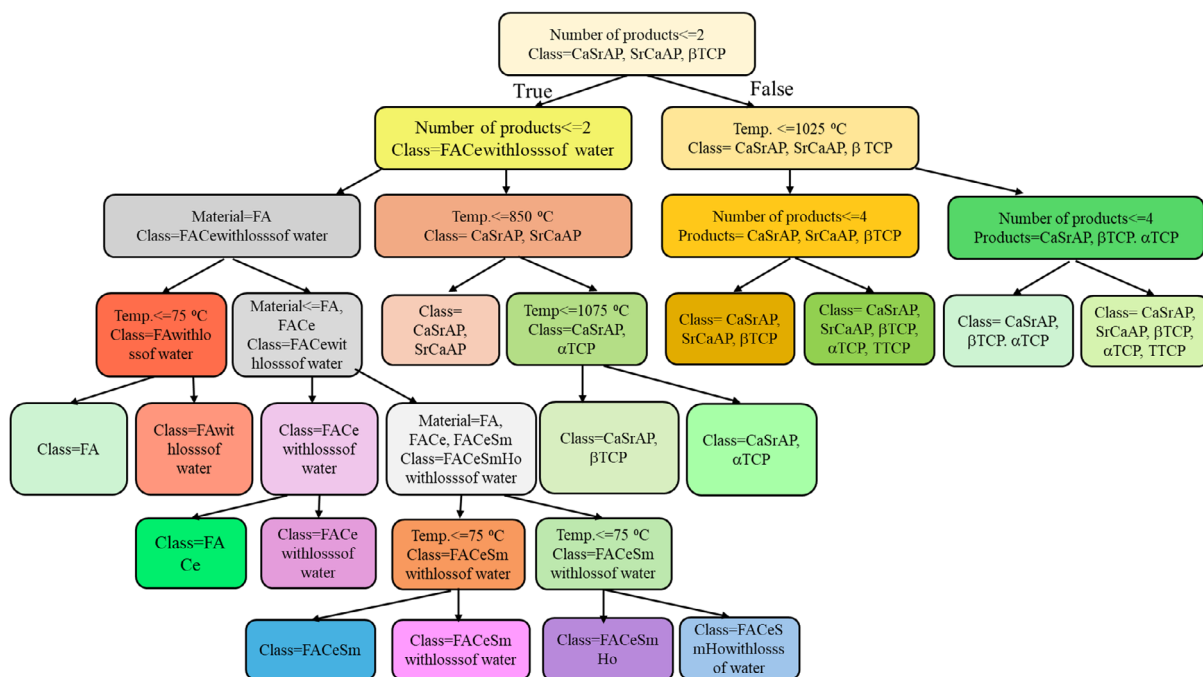

Figure 5. Decision tree classification of phase stability and decomposition behavior of rare-earth-doped apatite materials (FA, FACe, FACeSm, and FACeSmHo) in the temperature between 25 °C and 1200 °C. The model differentiates between stable and unstable phases, predicts phase transitions, and determines decomposition products like tri-calcium phosphates and apatite structures, as a function of material composition and temperature.

temperature, all of them get dehydrated upon heating. Near 600 °C, there is a critical phase transition that causes instability and creation of different decomposition products such as CaSrAP and SrCaAP. At temperatures above 650 °C, the system is more complicated, yielding extra calcium phosphate phases. At 1000 °C, products such as CaSrAP and α-TCP are created, which exhibit extra structural transformation.

The model discriminates between highly similar decomposition products due to temperature-driven transitions and dopant-specific chemical signatures. α-TCP and β-TCP, for example, are distinguished primarily due to their customary formation temperatures—β-TCP forms predominantly within the range 700–900 °C—while α-TCP forms at temperatures above 1100 °C. Such temperature thresholds constitute key decision nodes in the tree. Also, interactions between dopants govern phase selectivity; for instance, FACeSmHo composition has high correlation with TTCP formation above 1000 °C, suggesting that certain dopant combinations influence decomposition behavior. For complex multicationic phases like $Ca_{9.37}Sr_{0.63}(PO_4)_6(OH)_{0.98-2x}F_{0.02}O_x$, the model is based on stoichiometric trends (e.g., Sr/Ca ratios), the specific thermal window of stability (600–1200 °C), and co-occurrence patterns with phases like β-TCP. Correlation heatmap also support these model paths. This validate that the model is not entirely temperature reliant but accepts chemically meaningful patterns so that it can deconvolve phase superpositions. **Figure 6** shows the temperature trend and product formation with distinct single-phase stability at low temperatures to a more complex multiphase system at higher temperatures above 650 °C.

3.3. Influence of Multiple Oxidation States of Dopants on Phase Stability

The presence of multiple oxidation states of dopants such as cerium (Ce^{3+}/Ce^{4+}), samarium (Sm^{3+}/Sm^{2+}), and holmium (Ho^{3+}) ions significantly affect the thermal and phase stability properties of the apatite lattice. XPS analysis of the FACe system established that cerium exists as Ce^{3+} (36.5%) and Ce^{4+} (66.5%). The higher valency Ce^{4+} ions induce vacancy formation for charge compensation, and with heat treatment, further oxidation

of Ce^{3+} to Ce^{4+} increases the number of vacancies. These vacancies are known to induce phase transitions by localized rearrangements and induce phase separation, which tends to reduce structural stability.[28] In the FACeSm system, co-doping with samarium changes the redox balance: Ce^{3+} content increases to 47.7%, while samarium ion exists predominantly as Sm^{3+} (80.2%) with a smaller amount as Sm^{2+} (19.8%). Sm^{2+} increases (to 31.3%) when heated, but since Sm^{2+} is isovalent with Ca^{2+}, it does not create additional vacancies. The internal redox exchange between cerium and samarium ions reduces the vacancy concentration, leading to improved lattice stability and resistance to phase decomposition. On the other hand, holmium ion doping adds the single oxidation state Ho^{3+} only, as confirmed by XPS. While it does not form vacancies via redox processes, its very small ionic size induces lattice distortion, which can be responsible for phase instability upon thermal stress. Mixed-valent dopant ions like cerium and samarium regulate phase behavior primarily by vacancy formation, whereas Ho^{3+} does so by lattice distortion.

3.4. Thermodynamic Analysis of Phase Transitions in Apatite Materials

Gibbs free Energy calculations were done to understand the thermodynamics of phase transformations happening at various temperatures using Equation (1).[29,30] The calculated values of ΔG for each type of phase transition is calculated and listed in **Table 3**. The temperature-dependent-free energy change is controlling the phase transitions. All these transitions confirm to the key role of temperature-dependent free energy changes in controlling phase transformations. The adsorbed water is evaporated spontaneously as indicated by ΔG of −13.65 kJ mol⁻¹. A negative free energy change that promotes dehydration. At a temperature of 600 °C (873 K), formation of oxyapatite becomes thermodynamically favorable with a ΔG of −37.30 kJ mol⁻¹ leads to phase stabilization. At 800 °C (1073 K), spontaneous formation of β-TCP is supported by a ΔG of −53.76 kJ mol⁻¹, for its emergence as an intermediate phase. At 1000 °C (1273 K), the strongly negative ΔG of −100.95 kJ mol⁻¹ supports the formation of α-TCP and
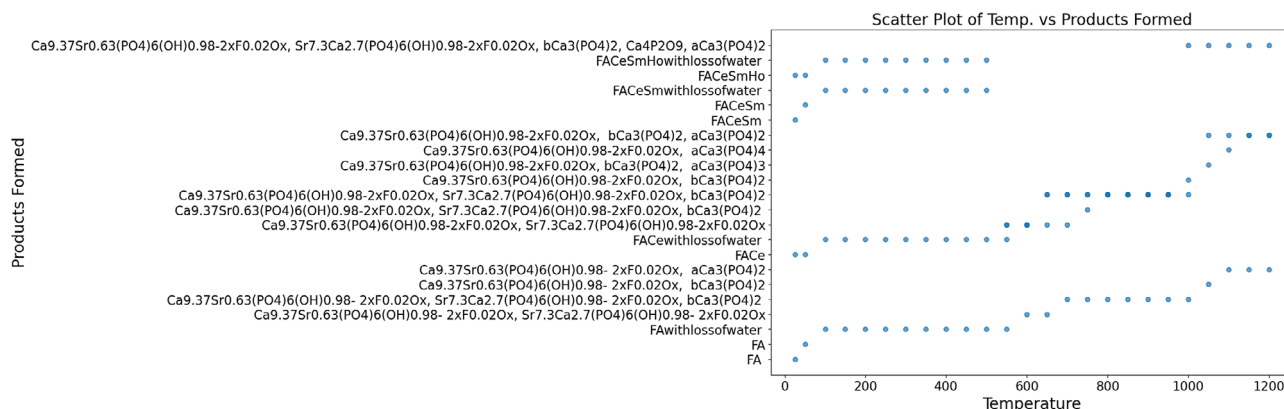

Figure 6. Scatter plot of the formation of various products as a function of temperature for four materials—FA, FACe, FACeSm, and FACeSmHo. The x-axis is the temperature range 25–1200 °C, and the y-axis is a list of phases that have been observed. The data points mark the onset of new phases and phase transitions with temperature increase, which illustrates the effect of rare-earth doping on thermal stability and decomposition pathway.

Table 3. Thermodynamic parameters (ΔH, ΔS, and ΔG) for phase transitions in apatite system at various temperatures. Negative ΔG values confirm the thermodynamic stability of each phase at its respective range of temperatures, with α-TCP and TTCP formation being the most spontaneous ($\Delta G = -100.95 \pm 4.61$ kJ mol^{-1} at 1000 °C).

Phase transition	Temperature [°C]	Temperature [K]	ΔH [kJ mol^{-1}]	ΔS [kJ mol·K^{-1}]	ΔG [kJ mol^{-1}]
Loss of absorbed water	200	473	10.00 ± 0.50	0.050 ± 0.01	-13.65 ± 2.42
Formation of oxyapatites	600	873	50.00 ± 0.85	0.100 ± 0.03	-37.30 ± 3.08
β-TCP ($Ca_3(PO_4)_2$)	800	1073	75.00 ± 1.24	0.120 ± 0.00	-53.76 ± 4.41
α-TCP ($Ca_3(PO_4)_2$) and TTCP ($Ca_4P_2O_9$)	1000	1273	90.00 ± 1.06	0.150 ± 0.04	-100.95 ± 4.61

TTCP, underlining their high-temperature thermodynamic stability. The change in the Gibbs free energy with temperature is shown in **Figure 7**.

$$\Delta G = \Delta H - T\Delta S \tag{1}$$

4. Usage of Decision Tree Classifier beyond 1200 °C

The decision tree model was employed to predict the thermal stability of doped apatite systems at elevated temperatures of 1300 and 1500 °C. The decision tree yielded an accuracy of 1 for these temperatures. The predicted phase transformations and decomposition trends showed strong agreement with previously reported experimental findings. Chun-Jen Liao et al., investigated the thermal decomposition of apatites up to 1500 °C and reported the formation of secondary phases such as tetra calcium phosphate (TTCP) and tricalcium phosphate (TCP), consistent with our model's projection of apatite breakdown and multiphase formation at high temperatures.[31] Similarly, Makarova et al. demonstrated that Fe and Si co-doping induces phase instability and dopant segregation at higher concentrations, leading to the

formation of non-apatites calcium phosphate phases—an effect also captured by our model.[32] These comparisons support the model's capacity to reliably extrapolate phase stability and compositional behavior of doped apatite systems beyond experimentally explored temperature regimes.

5. Conclusions

Herein, the successful incorporation of a ML approach with traditional but necessary experimental phase transformation characterization methods is illustrated. The work aimed to analyze the means and methods of phase stability enhancement in rare-earth ion-doped apatite materials. The phase decomposition and stability behavior of some apatite compositions in the wide temperature between 25 °C and 1200 °C were predicted using a decision tree model. Clearly defined stable and unstable regimes were observed, along with phase transitions at the critical point of about 600 °C. Single-phase material dominated the stable regime, but instability was succeeded by a complicated mixture of various decomposition products, such as tri-calcium phosphates and apatite structures. The HT-XRD and TGA data sets collected were extremely helpful in training the ML model, which was found to predict phase stability and product formation accurately (≈86%). This work demonstrates the capability of ML in the field of materials science, focusing on material composition and discovery optimization for desired thermal properties. The study not only improves the understanding of apatite structures but also paves the way for the development of high-temperature applications and new material synthesis in future studies.

Supporting Information

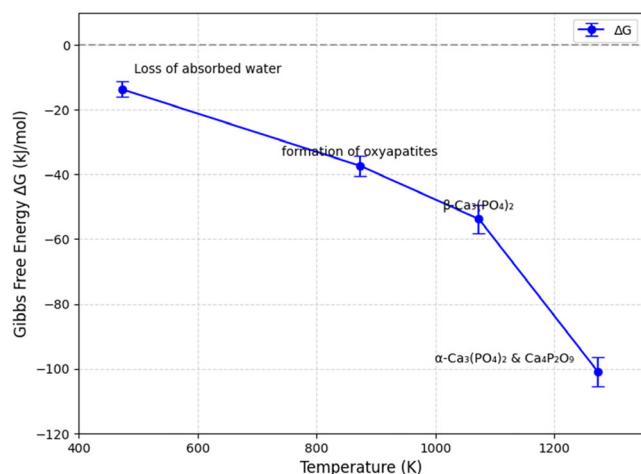Supporting Information is available from the Wiley Online Library or from the author.

Figure 7. Gibbs free energy change (ΔG) of phase transitions as a function of temperature (K). The graph represents the temperature ranges over which each phase becomes thermodynamically stable, as indicated by negative ΔG values. The data indicate the thermodynamic favorability of the processes, with more negative ΔG values indicating greater spontaneity under the conditions.

**ADVANCED
SCIENCE NEWS**

www.advancedsciencenews.com

**ADVANCED
INTELLIGENT
SYSTEMS**
Open Access

www.advintellsyst.com

Conflict of Interest

The authors declare no conflict of interest.

Author Contributions

Geeta Sharma: conceptualization (lead); data curation (lead); formal analysis (lead); funding acquisition (equal); investigation (lead); methodology (lead); and writing—original draft (lead). **Sarathkumar Loganathan:** methodology (supporting). **Evangelos Daskalakis:** data curation (supporting). **Eric K. Barimah:** data curation (supporting). **Simon Strafford:** data curation (supporting). **Animesh Jha:** supervision (lead) and writing—review and editing (supporting).

Data Availability Statement

The data that support the findings of this study are available from the corresponding author upon reasonable request.

Keywords

[1] Y. Waseda, M. Masuda, K. Watanabe, H. Shibata, H. Ohta, K. Nakajima, *High Temp. Mater. Processes* **1994**, *13*, 267.

[2] M. Pasero, A. R. Kampf, C. Ferraris, I. V. Pekov, J. Rakovan, T. J. White, *Euro. J. Mineral.* **2010**, *22*, 163.

[3] G. Sharma, S. Loganathan, E. K. Barimah, P. Georgopoulou, E. Taylor, A. J. Scott, S. Strafford, A. Jha, *ChemPhysChem* **2024**, *25*, 202400109.

[4] C. L. Owens, G. R. Nasha, K. Hadler, R. S. Fitzpatrick, C. G. Anderson, F. Wall, *Adv. Colloid Interface Sci.* **2019**, *265*, 14.

[5] S. V. Dorozhkin, *Materials* **2009**, *2*, 399.

[6] R. Rial, M. González-Durruthy, Z. Liu, J. M. Ruso, *Molecules* **2021**, *26*, 3190.

[7] K. Tõnsuaadu, K. A. Gross, L. Pluduma, M. Veiderma, *J. Thermal Anal. Calorimetry* **2012**, *110*, 647.

[8] N. Leroy, E. Bres, D. B. Jones, S. Downes, *Euro. Cells Mater.* **2001**, *2*, 36.

[9] J. M. Hughes, D. Harlov, J. F. Rakovan, *Am. Mineral.* **2018**, *103*, 1981.

[10] M.-E. Fleet, Y. Pan, *Am. Mineral.* **1995**, *80*, 329.

[11] K. A. Gschneidner, L. Eyring, *Handbook on the Physics and Chemistry of Rare Earths*, Elsevier Science Publishers B.V., North-Holland **1993**.

[12] P. K. Sahu, M. Ramrakhiani, S. Agrawal, *J. Fluoresc.* **2019**, *29*, 1249.

[13] S. Ferraris, S. Yamaguchi, N. Barbani, C. Cristallini, G. G. di Confiengo, J. Barberi, M. Cazzola, M. Miola, E. Vernè, S. Spriano, *Mater. Sci. Eng. C* **2020**, *116*, 111238.

[14] N. V. Bulina, S. V. Makarova, S. G. Baev, A. A. Matvienko, K. B. Gerasimov, O. A. Logutenko, V. S. Bystrov, *Minerals* **2021**, *11*, 1310.

[15] Y. Chen, X. Miao, *Biomaterials* **2005**, *26*, 2105.

[16] A. V. Knyazev, E. N. Bulanov, V. Z. Korokin, *Mater. Res. Bull.* **2015**, *61*, 47.

[17] N. G. Chernorukov, A. V. Knyazev, E. N. Bulanov, *Inorg. Mater.* **2011**, *47*, 127.

[18] A. D. Anastasiou, M. Nerantzaki, E. Gounari, M. S. Duggal, P. V. Giannoudis, A. Jha, D. Bikiaris, *Sci. Rep.* **2019**, *9*, 14469.

[19] K. T. Butler, D. W. Davies, H. Cartwright, O. Isayev, A. Walsh, *Nature* **2018**, *559*, 547.

[20] T. Lookman, P. V. Balachandran, D. Xue, R. Yuan, *npj Comput. Mater.* **2019**, *18*, 21.

[21] R. Ramprasad, R. Batra, G. Pilania, A. Mannodi-Kanakkithodi, C. Kim, *npj Comput. Mater.* **2017**, *3*, 54.

[22] B. Kovalerchuk, A. Dunn, A. Worland, S. Wagle, *Interactive Decision Tree Creation and Enhancement with Complete Visualization for Explainable Modeling.* In: B. Kovalerchuk, K. Nazemi, R. Andonie, N. Datia, E. Banissi (eds) *Artificial Intelligence and Visualization: Advancing Visual Knowledge Discovery. Studies in Computational Intelligence, vol 1126.* Springer, Cham **2024**, pp. 3–40.

[23] H. Blockeel, L. Devos, B. Frénay, G. Nanfack, S. Nijssen, *Front. Artificial Intell.* **2023**, *6*, 1124553.

[24] K. M. Ali, *IgMin Res.* **2024**, *2*, 425.

[25] S. Uddin, I. Haque, H. Lu, M. A. Moni, E. Gide, *Sci. Rep.* **2022**, *12*, 6256.

[26] G. S. Priyanga, S. Sampath, P. V. Shravan, R. N. Sujith, A. M. Javeed, G. Latha, *Solar Energy* **2024**, *278*, 112782.

[27] N. Nagappan, G. S. Priyanga, T. Thomas, *Phys. B: Condensed Matter* **2025**, *696*, 416638.

[28] J.-M. Liu, *Scr. Mater.* **1997**, *37*, 535.

[29] R. A. Robie, D. R. Waldbaum, *Thermodynamic Properties of Minerals and Related Substances at 298.15° K (25.0° C) and One Atmosphere (1.013 Bars) Pressure and at Higher Temperatures* **1968**, U.S. Geological Survey, https://i-share-eiu.primo.exlibrisgroup.com/permalink/01CARLI_EIU/7gt4dg/alma9914168255205833 (accessed: 2025).

[30] F. J. A. L. Cruz, M. E. Minas Da Piedade, J. C. G. Calado, *J. Chem. Thermodyn.* **2005**, *37*, 1061.

[31] C.-J. Liao, F.-H. Lin, K.-S. Chen, J.-S. Sun, *Biomaterials* **1999**, *20*, 1807.

[32] S. V. Makarova, N. V. Bulina, O. B. Vinokurova, A. V. Ishchenko, *Powders* **2023**, *2*, 372.